Research Article Vol. 30, No. 2 / 17 Jan 2022 / Optics Express 3047
Optics EXPRESS

Near 100% external quantum efficiency 1550-nm broad spectrum photodetector

YANG SHEN,[1] XINGJUN XUE,[1] ANDREW H. JONES,[1] YIWEI PENG,[1] JUNYI GAO,[1] TA CHING TZU,[1] MATT KONKOL,[2] AND JOE C. CAMPBELL[1,*]

[1]*Department of Electrical and Computer Engineering, University of Virginia, Charlottesville, VA 22904, USA*
[2]*Phase Sensitive Innovations, 51 East Main Street, Suite 201, Newark, DE 19711, USA*
[*]*jcc7s@virginia.edu*

Abstract: We report InGaAs/InP based p-i-n photodiodes with an external quantum efficiency (EQE) above 98% from 1510 nm to 1575 nm. For surface normal photodiodes with a diameter of 80 μm, the measured 3-dB bandwidth is 3 GHz. The saturation current is 30.5 mA, with an RF output power of 9.3 dBm at a bias of −17 V at 3 GHz.

1. Introduction

High quantum efficiency and high-speed photodiodes play a vital role in quantum information and quantum optical systems [1–6]. Photo-count statistics give a true measure of incoming photon statistics, with a fidelity that increases as the efficiency of the detector increases [7]. Such a task cannot be realized by detectors with an internal gain such as a single-photon avalanche detector (SPAD) or a photomultiplier tube (PMT), since the multiplication process disrupts the photon statistics of the signal [8,9].

The most straightforward method to increase quantum efficiency is to simply increase the thickness of the absorber [10]. However, thick absorbers will increase the transit time of the carriers, thus decreasing the speed of the detector. Therefore, as determined by the application, it is important to design the structure to achieve the optimum efficiency/bandwidth tradeoff at the operating wavelength. It is also important to incorporate a high-quality anti-reflection coating to eliminate photon loss due to light reflection or scattering.

Extensive work has been devoted to improving the speed, linearity, and power handling capability of photodetectors that operate in the telecommunication band, but the EQE of these detectors is rarely the primary focus [11–16]. To reach 100% EQE at 1550 nm, the responsivity of the detectors must be close to 1.26 A/W. Most reported InGaAs-based photodiodes have a responsivity of less than 1.1 A/W [17–20], which is equivalent to 87.6% EQE. In this letter, we report high quantum efficiency p-i-n photodiodes that achieve 98% detection efficiency at 1550 nm. For 80-μm-diameter devices, the 3-dB bandwidth is 3 GHz, which is RC-limited.

2. Device design and fabrication

The near 100% EQE photodiodes that operate at 1550 nm are realized with a surface-normal backside-illuminated photodiode design. Multiple photon loss mechanisms are addressed in this design as shown in Fig. 1. First, the backside of the detector is polished and an anti-reflection coating is applied to eliminate scattering and reflection loss at the air-detector interface. Second, InP provides an ideal substrate as it is transparent at the designed wavelength. Third, 4 μm of unintentionally-doped $In_{0.53}Ga_{.047}As$ was chosen as the absorption layer. Given an absorption coefficient of 0.619 μm^{-1} [21], a single pass through the 4-μm-thick InGaAs layer will result in 91.6% absorption of the incident light, while a double pass assuming perfect reflection at the

#447091 https://doi.org/10.1364/OE.447091
Journal © 2022 Received 28 Oct 2021; revised 18 Nov 2021; accepted 25 Nov 2021; published 14 Jan 2022

Optics EXPRESS

top metal contact results in 99.3% absorption of the incident light that enters the photodiode. The absorption layer has to be thick enough to capture almost all of the photons, yet not so thick that the carriers recombine before collection. Lastly, to ensure the highest reflection between top metal contact layer and P-layer, silver is used beneath the gold contact surface to replace the traditional adhesion metal, titanium, which increases the reflectivity of the InGaAsP-metal interface from 28% to 93% at 1550 nm. The estimated EQE of the photodiode that use silver as the adhesion layer is 98.7%, while the EQE will be only 93.8% if titanium is used as the adhesion layer.

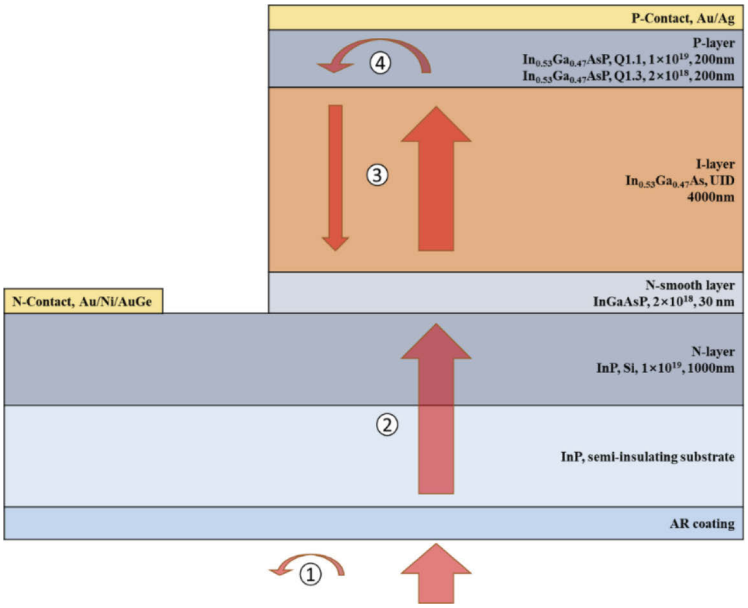

Fig. 1. Structure of the 1550 nm high quantum efficiency photodetector.

The detailed epitaxial-layer structure of the photodiode is shown in Fig. 1. The epitaxial-layers are grown on a semi-insulating InP substrate by metal organic chemical vapor deposition. Silicon and zinc are used as n-type and p-type dopants, respectively. The 200-nm p-contact layer is heavily p-doped (1×10^{19} cm^{-3}) InGaAsP. This is followed by a 200-nm p-doped (2×10^{18} cm^{-3}) InGaAsP layer and the unintentionally doped $In_{0.53}Ga_{0.47}As$ absorber. A 30-nm-thick InGaAsP grading layer is placed under the absorption layer to smooth the heterojunction discontinuity with InP. This followed by 1 µm of n-doped (1×10^{19} cm^{-3}) InP as the n-contact layer.

The fabrication process begins with the deposition of the highly reflective p contact metal layer. A metal stack of 20-nm Ag and 150-nm Au is deposited on the p-type InGaAsP contact layer by electron beam evaporation. Inductively coupled plasma (ICP) dry etching is used to form the mesa of the photodiode. The dry etching stops at the highly doped n-contact layer. This is followed by the n-contact metal deposition. To reduce the scattering and reflection at the semiconductor/air interface, the backside of the device is first polished and then coated with an anti-reflection layer. The anti-reflection coating is deposited by Evaporated Coatings Inc. As shown in Fig. 2, the reflectivity is less than 0.1% at 1550 nm.

Optics EXPRESS

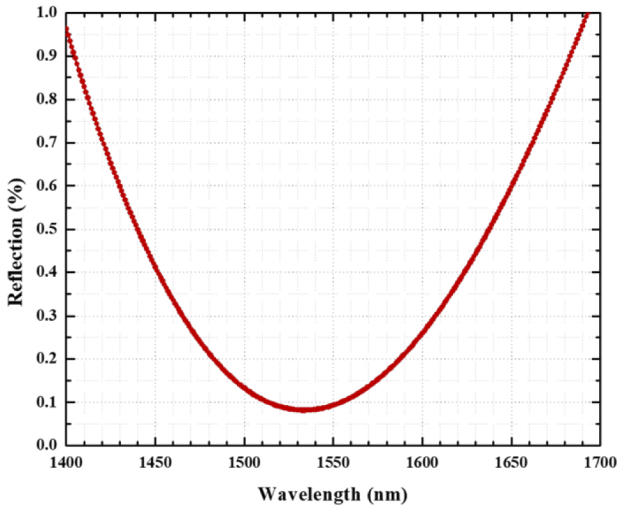

Fig. 2. Measured reflection versus wavelength after deposition of the anti-reflection coating.

3. Results and discussion

3.1. Quantum efficiency

Figure 3 shows the experimental setup for the EQE measurements. A high-pressure laser-driven lamp is used as a broadband white light source. A SPEX 1681 monochromator filters the incident wavelength. The selected light is collimated and focused on the backside of the photodiodes. A chopper is placed after the monochromator to provide intensity modulation (200-300 Hz). Finally, the photocurrent is measured by a Stanford Research SR-850 lock-in amplifier. The EQE is obtained by comparing the measured photo response of the device to that of a photodetector with a calibrated responsivity.

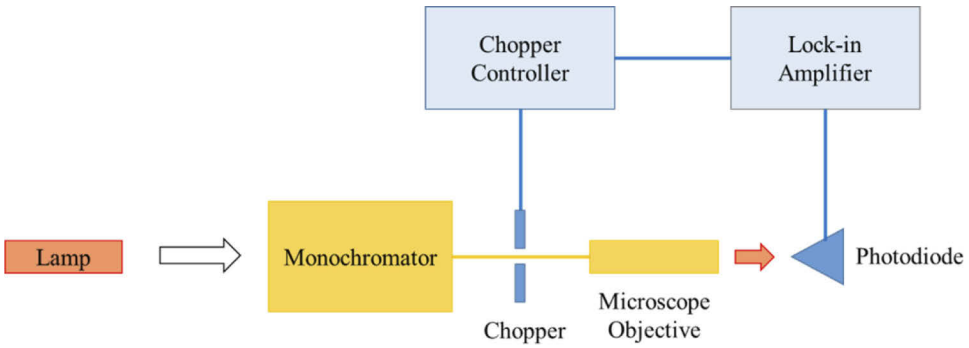

Fig. 3. Quantum efficiency measurement setup.

Devices with diameters ranging from 80 μm to 500 μm were fabricated. All devices show nearly the same EQE. Figure 4(a) shows the measured EQE of a 150-μm-diameter device. As shown in the figure, three EQE measurements were separately conducted at - 5 V bias during different stages of the fabrication process. The lowest one is recorded before the backside of the device was polished. Approximately 50% of the light is either reflected or scattered. After the substrate was polished, the EQE increased by 20% due to the elimination of scattering. Finally, with an anti-reflection coating, the EQE increased to > 98% from 1510 nm to 1575 nm as shown

Optics EXPRESS

in Fig. 4(b). At 1550 nm, the measured EQE is 98.3%. As explained in the calculation in section 2, the 1~2% loss is very likely coming from two parts: loss due to reflection loss at top metal contact layer and P-layer interface, and loss due the limited thickness of the absorption layer.

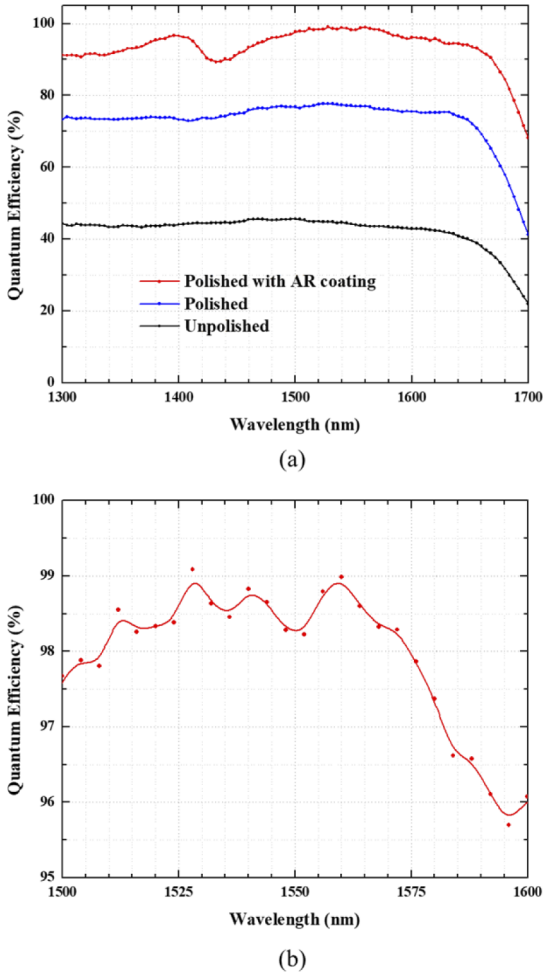

Fig. 4. (a) Measured EQE of a 150-μm-diameter device before backside polishing, after backside polishing, and after deposition of an anti-reflection coating. (b) Measured EQE of a 150-μm-diameter device from 1500 nm to 1600 nm.

The EQE quickly decreases beyond ~1650 nm as the optical cutoff of $In_{0.53}Ga_{0.47}As$ is approached.

Figure 5 shows the quantum efficiency (red curve) and capacitance (blue curve) of a 150-μm-diameter device versus reverse bias. The quantum efficiency reaches it maximum and the saturates at – 2 V. This indicates that the device is fully depleted at this voltage, resulting in efficient collection of photogenerated carriers.

3.2. Bandwidth

Figure 6 shows the bandwidth measurement setup. The light from a 1550 nm external cavity laser is directly modulated by an optical modulator. The optical signal is then amplified by an erbium doped fiber amplifier (EDFA) before being coupled into the device through a lensed fiber.

Optics EXPRESS

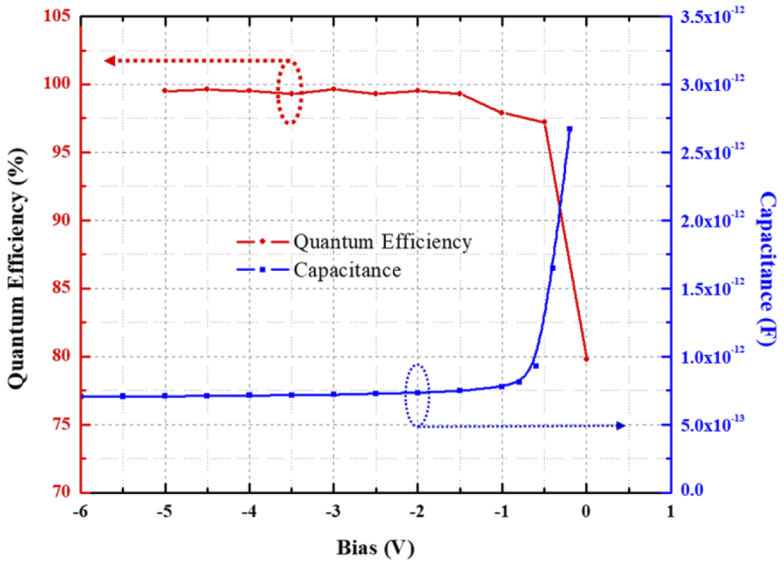

Fig. 5. Measured EQE of a 150-μm-diameter device at bias range from 0 V to −5 V reverse bias in 0.5 V increments.

The bias voltage of the device is supplied by a source meter through a bias tee. The output RF power of the device is measured by an RF power meter.

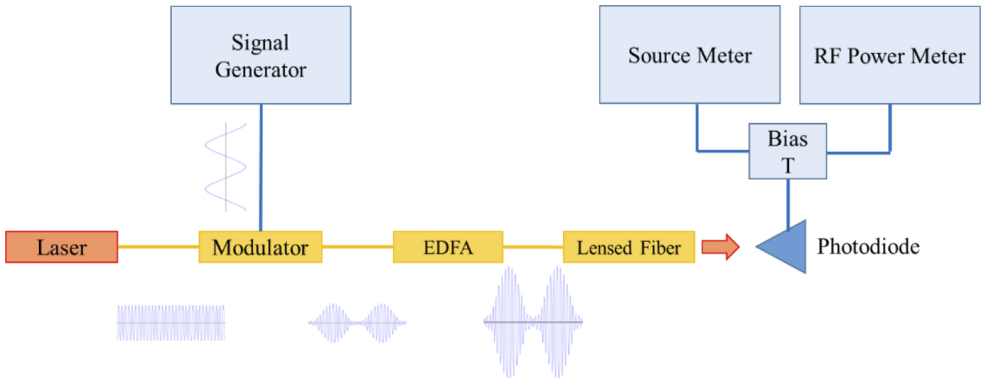

Fig. 6. Bandwidth measurement setup.

As shown in Fig. 7(a), the frequency responses of the photodiodes decrease quickly as the diameter of the devices increase from 80 μm to 500 μm. The measured 3-dB bandwidths are 3 GHz, 1.8 GHz, 1.2 GHz, 0.8 GHz, and 0.5 GHz for photodiodes with diameters of 80 μm, 200 μm, 250 μm, 350 μm, and 500 μm, respectively. The strong bandwidth dependence on diameter indicates that the 3-dB bandwidth is dominated by the RC time response. The bias dependence of the bandwidth for a 150-μm photodiode is shown in Fig. 7(b). The bandwidth increases from 1 GHz at −1 V to almost 2 GHz at −5 V bias.

Figure 8(a) shows the calculated transit-time-limited and RC-limited bandwidth components for device diameters ranging from 80 μm to 500 μm at a bias voltage of −5 V. The transit-time-limited bandwidth is 5.5 GHz, while, as expected, the RC-limited bandwidth varies with the device area. The RC-limited bandwidth was calculated using the measured series resistance and capacitance

Optics EXPRESS

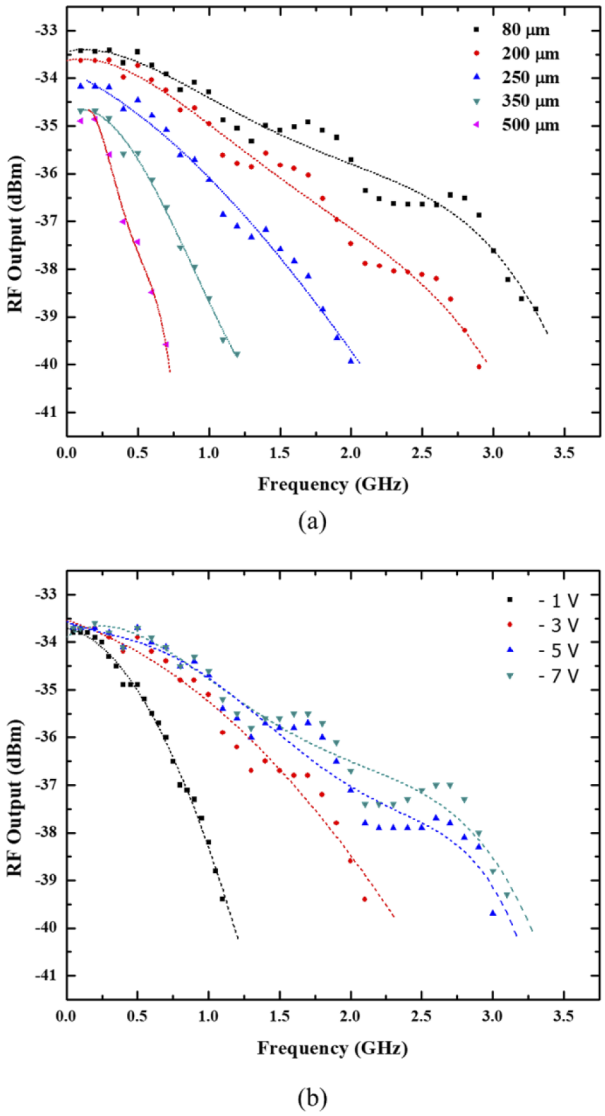

Fig. 7. (a) Frequency responses of the photodiodes with diameters ranging from 80 μm to 500 μm at a bias voltage of −5 V. (b) Frequency responses of the 150-μm photodiodes with biases ranging from −1 V to −7 V.

of the devices. Figure 8(b) shows the calculated and measured bandwidth for device diameters ranging from 80 μm to 500 μm at bias voltage of −5 V. The calculated bandwidths agree well with the measured.

3.3. Saturation

The saturation current, or the 1-dB compression current, is defined as the time-average photocurrent at which the RF output power is 1 dB lower than the output power predicted by the time-average photocurrent. It indicates the maximum photocurrent that can be sustained by the device before it can no longer linearly transform the waveform of the optical signal. The measurement setup is similar to the bandwidth setup, light from two lasers with wavelength near

Optics EXPRESS

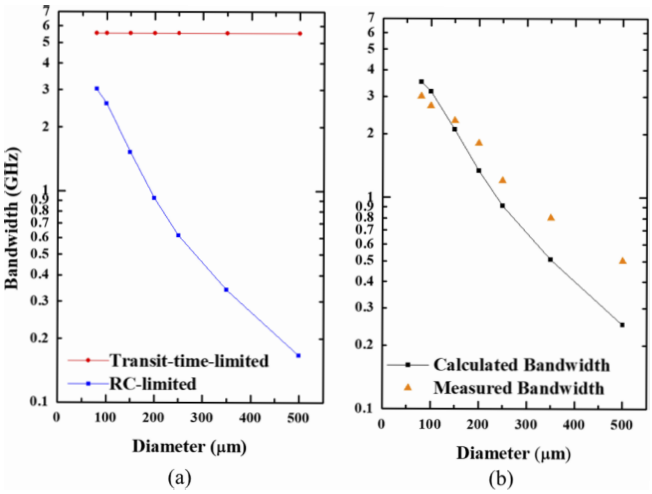

Fig. 8. (a) Calculated transit-time-limited bandwidth and RC-limited bandwidth of the photodiodes. (b) Comparison of calculated and measured bandwidth versus diameter at a bias voltage of −5 V.

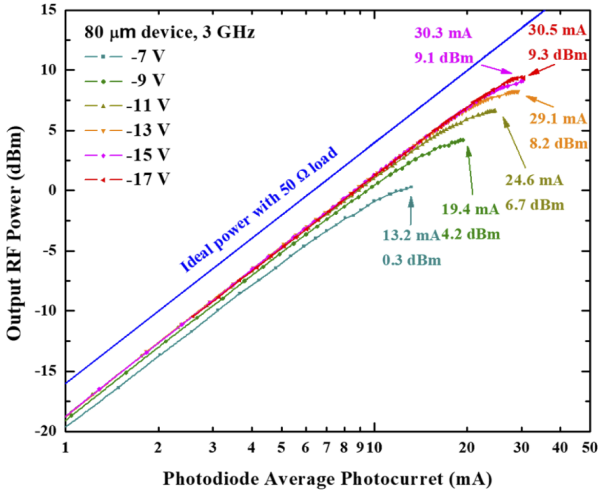

Fig. 9. RF output power of a 80-μm device as a function of photocurrent at 3 GHz.

1550 nm were used to generate a frequency-swept beat signal with ~100% modulation depth, and the RF output of the device is recorded with its corresponding photocurrent. As shown in Fig. 9, an 80-μm device shows a saturation current of 30.5 mA, with an RF output of 9.3 dBm at a bias of −17 V at 3 GHz. At low biases, the saturation of the photocurrent is caused by the self-induced field as they are retractable after 1-dB compression. However, at bias higher than 17 V, the devices are more easily to experience irreversible thermal breakdown when approaching compression, with little enchantment in its maximum RF output power.

4. Conclusion

In this letter, we report p-i-n photodiodes with 98.3% EQE at 1550 nm. To achieve high EQE, a 4-μm-thick absorber and a double-pass architecture were utilized to fully absorb the light.

Optics EXPRESS

Surface polishing and an anti-reflection coating effectively reduced the scattering and reflection at the semiconductor/air interface. At a bias of −5 V, the 3-dB bandwidth was 3 GHz and the saturation current was 30.5 mA with an RF output power of 9.3 dBm.

Funding. National Science Foundation (1838435, 1839175).

Disclosures. The authors declare no conflicts of interest.

Data Availability. Data underlying the results presented in this paper are not publicly available at this time but may be obtained from the authors upon reasonable request.

References

1. V. D. Vaidya, B. Morrison, L. G. Helt, R. Shahrokshahi, D. H. Mahler, M. J. Collins, K. Tan, J. Lavoie, A. Repingon, M. Menotti, N. Quesada, R. C. Pooser, A. E. Lita, T. Gerrits, S. W. Nam, and Z. Vernon, "Broadband quadrature-squeezed vacuum and nonclassical photon number correlations from a nanophotonic device," Sci. Adv. **6**(39), eaba9186 (2020).
2. Y. Zhao, Y. Okawachi, J. K. Jang, X. Ji, M. Lipson, and A. L. Gaeta, "Near-Degenerate Quadrature-Squeezed Vacuum Generation on a Silicon-Nitride Chip," Phys. Rev. Lett. **124**(19), 193601 (2020).
3. M. Pysher, R. Bloomer, C. M. Kaleva, T. D. Roberts, P. Battle, and O. Pfister, "Broadband amplitude squeezing in a periodically poled KTiOPO4 waveguide," Opt. Lett. **34**(3), 256–258 (2009).
4. R. Bloomer, M. Pysher, and O. Pfister, "Nonlocal restoration of twomode squeezing in the presence of strong optical loss," New J. Phys. **13**(6), 063014 (2011).
5. M. Chen, N. C. Menicucci, and O. Pfister, "Experimental Realization of Multipartite Entanglement of 60 Modes of a Quantum Optical Frequency Comb," Phys. Rev. Lett. **112**(12), 120505 (2014).
6. H. Vahlbruch, M. Mehmet, K. Danzmann, and R. Schnabel, "Detection of 15 dB squeezed states of light and their application for the absolute calibration of photoelectric quantum efficiency," Phys. Rev. Lett. **117**(11), 110801 (2016).
7. M. Fox, *Quantum Optics: An Introduction*. Oxford University Press, New York, NY, USA, 2006, pp. 93.
8. R. H. Hadfield, "Single-photon detectors for optical quantum information applications," Nat. Photonics **3**(12), 696–705 (2009).
9. T. Shima and Y. Nagai, "Development of a photomultiplier tube with high quantum efficiency," Nucl. Instrum. Methods Phys. Res. **431**(1-2), 185–193 (1999).
10. X. Li, N. Li, S. Demiguel, X. Zheng, J. C. Campbell, H. H. Tan, and C. Jagadish, "A partially depleted absorber photodiode with graded doping injection regions," IEEE Photonics Technol. Lett. **16**(10), 2326–2328 (2004).
11. T. Ishibashi, S. Kodama, N. Shimizu, and T. Furuta, "High-speed response of uni-traveling-carrier photodiodes," Jpn. J. Appl. Phys. **36**(Part 1, No. 10), 6263–6268 (1997).
12. T. Shi, B. Xiong, C. Sun, and Y. Luo, "Novel back-to-back uni-traveling carrier photodiodes with high responsivity and wide bandwidth," in *Proc. Opt. Fiber Commun. Conf.*, 2013, p. OW3J.2.
13. X. Xie, Q. Zhou, E. Norberg, M. Jacob-Mitos, Y. Chen, A. Ramaswamy, G. Fish, J. E. Bowers, J. C. Campbell, and A. Beling, "Heterogeneously integrated waveguide-coupled photodiodes on SOI with 12 dBm output power at 40 GHz," in *Proc. Opt. Fiber Commun. Conf.*, 2015, p. Th5B.7.
14. Y. Peng, K. Sun, Y. Shen, A. Beling, and J. C. Campbell, "High-Power and High-Linearity Photodiodes at 1064 nm," J. Lightwave Technol. **38**(17), 4850–4856 (2020).
15. Y. Peng, J. Zang, K. Sun, Z. Yang, and J. C. Campbell, "High-Speed and High-Power MUTC Photodiode Working at 1064 nm," IEEE Photonics Technol. Lett. **31**(19), 1584–1587 (2019).
16. Y. Peng, K. Sun, Y. Shen, A. Beling, and J. C. Campbell, "Photonic generation of pulsed microwave signals in the X-, Ku-and K-band," Opt. Express **28**(19), 28563–28572 (2020).
17. J. C. Campbell, A. Dentai, T. Lee, and C. Burrus, "Improved two-wavelength demultiplexing InGaAsP photodetector," IEEE J. Quantum Electron. **16**(6), 601–603 (1980).
18. I. Kimukin, N. Biyikli, B. Butun, O. Aytur, S. M. Unlu, and E. Ozbay, "InGaAs-based high-performance p-i-n photodiodes," IEEE Photonics Technol. Lett. **14**(3), 366–368 (2002).
19. Q. Yu, K. Sun, Q. Li, and A. Beling, "Segmented waveguide photodetector with 90% quantum efficiency," Opt. Express **26**(10), 12499–12505 (2018).
20. B. Song, B. Shi, S. Š. Brunelli, and J. Klamkin, "InGaAs Photodiode Array on Silicon by Heteroepitaxy," in *Conference on Lasers and Electro-Optics*, J. Kang, S. Tomasulo, I. Ilev, D. Müller, N. Litchinitser, S. Polyakov, V. Podolskiy, J. Nunn, C. Dorrer, T. Fortier, Q. Gan, and C. Saraceno, eds., OSA Technical Digest (Optical Society of America, 2021), paper STh2H.2.
21. S. Adachi, "Optical dispersion relations for GaP, GaAs, GaSb, InP, InAs, InSb, $Al_xGa_{1-x}As$, and $In_{1-x}Ga_xAs_yP_{1-y}$," J. Appl. Phys. **66**(12), 6030–6040 (1989).